THE JOURNAL OF BIOLOGICAL CHEMISTRY VOL. 287, NO. 8, pp. 5650–5660, February 17, 2012

Structural Basis for Increased Toxicity of Pathological $A\beta_{42}$:$A\beta_{40}$ Ratios in Alzheimer Disease*[S]

Received for publication, May 25, 2011, and in revised form, November 30, 2011 Published, JBC Papers in Press, December 8, 2011, DOI 10.1074/jbc.M111.264473

Kris Pauwels[‡1], Thomas L. Williams[§2,3], Kyle L. Morris[§], Wim Jonckheere[¶‖], Annelies Vandersteen[¶‖4], Geoff Kelly[‡], Joost Schymkowitz[¶‖], Frederic Rousseau[¶‖], Annalisa Pastore[‡], Louise C. Serpell[§3], and Kerensa Broersen[¶‖5]

From the [‡]Division of Molecular Structure, Medical Research Council National Institute for Medical Research, The Ridgeway, Mill Hill, London NW7 1AA, United Kingdom, the [§]School of Life Sciences, University of Sussex, Falmer, East Sussex BN1 9QJ, United Kingdom, the [¶]Switch Laboratory, Flanders Institute for Biotechnology (VIB), Pleinlaan 2, 1050 Brussels, Belgium, and the [‖]Vrije Universiteit Brussel, Pleinlaan 2, 1050 Brussels, Belgium

Background: Amyloid β peptide plays a role in Alzheimer disease.
Results: Interaction of amyloid β peptides with 40 and 42 amino acids has consequences for oligomer formation.
Conclusion: Increased production of amyloid β peptide with 42 amino acids affects the behavior of the entire amyloid β peptide pool.
Significance: This might explain the synaptotoxic effect observed with a shift in amyloid β peptide production.

The β-amyloid peptide ($A\beta$) is directly related to neurotoxicity in Alzheimer disease (AD). The two most abundant alloforms of the peptide co-exist under normal physiological conditions in the brain in an $A\beta_{42}$:$A\beta_{40}$ ratio of ~1:9. This ratio is often shifted to a higher percentage of $A\beta_{42}$ in brains of patients with familial AD and this has recently been shown to lead to increased synaptotoxicity. The molecular basis for this phenomenon is unclear. Although the aggregation characteristics of $A\beta_{40}$ and $A\beta_{42}$ individually are well established, little is known about the properties of mixtures. We have explored the biophysical and structural properties of physiologically relevant $A\beta_{42}$:$A\beta_{40}$ ratios by several techniques. We show that $A\beta_{40}$ and $A\beta_{42}$ directly interact as well as modify the behavior of the other. The structures of monomeric and fibrillar assemblies formed from $A\beta_{40}$ and $A\beta_{42}$ mixtures do not differ from those formed from either of these peptides alone. Instead, the co-assembly of $A\beta_{40}$ and $A\beta_{42}$ influences the aggregation kinetics by altering the pattern of oligomer formation as evidenced by a unique combination of solution nuclear magnetic resonance spectroscopy, high molecular weight mass spectrometry, and cross-seeding experiments. We relate these observations to the observed enhanced toxicity of relevant ratios of $A\beta_{42}$:$A\beta_{40}$ in synaptotoxicity assays and in AD patients.

Alzheimer disease (AD)[6] is a multifactorial neurodegenerative disease that mainly affects the growing population of the elderly. The primary agents of AD, the β-amyloid peptides ($A\beta$), are produced from the amyloid precursor protein by sequential endoproteolytic cleavages. The severity of dementia correlates with soluble assemblies of $A\beta$ peptides rather than with the final fibrillar $A\beta$ deposits observed in the brain (1) and a plethora of different toxic oligomers have been identified (2–5).

Imprecise cleavage of the amyloid precursor protein substrate by γ-secretase or altered catabolism of the $A\beta$ peptides affect the relative amounts of $A\beta_{42}$ and $A\beta_{40}$, the two main $A\beta$ fragments (6–8). An increased $A\beta_{42}$:$A\beta_{40}$ ratio seems to coincide with more aggressive forms of the disease compared with cases of sporadic AD (9) and affects synaptic activity, viability of neuronal cells, and memory formation in animals (7, 8, 10–12). Recently, minor shifts in the $A\beta_{42}$:$A\beta_{40}$ ratio have been reported to drastically influence the formation of neurotoxic oligomers (13, 14). Despite the very similar chemical nature of the two peptides, they seem to have quite different structural and biophysical properties. $A\beta_{42}$ is known to be highly fibrillogenic and more prone than $A\beta_{40}$ to form neurotoxic assemblies (13, 15–17). Different architectures of *in vitro*-generated amyloid fibrils from pure $A\beta_{40}$ and $A\beta_{42}$ peptides have been revealed by nuclear magnetic resonance (NMR) (18), electron microscopy (EM) (19), and x-ray fiber diffraction methods (20–22). A limited number of studies have demonstrated that $A\beta_{40}$ and $A\beta_{42}$ each affect the aggregation rates of the other, and it is generally reported that $A\beta_{40}$ inhibits the aggregation of $A\beta_{42}$ (12, 14, 23–27).

To date, most structural and biophysical studies have been performed using $A\beta_{40}$ or $A\beta_{42}$ in isolation. However, the aberrant behavior of neurotoxic $A\beta$ peptides directed by the $A\beta_{42}$:$A\beta_{40}$ ratio requires the need to simultaneously investigate $A\beta_{40}$

* This work was supported in part by the Fund for Scientific Research Flanders, the Federal Office for Scientific Affairs, Belgium IUAP P6/43, Alzheimer's Research UK, the Research Foundation–Flanders (FWO), Stichting Alzheimer Onderzoek (SAO), and the FWO Odysseus Program.
[S] This article contains supplemental Table S1 and Figs. S1 and S2.
[1] Recipient of a European Molecular Biology Organization long term postdoctoral fellowship (ALTF 512-2008).
[2] Present address: Dept. of Physics 12-908, Drexel University, 3141 Chestnut St., Philadelphia, PA 19104.
[3] Supported by Alzheimer's Research UK.
[4] Supported by an agency for Innovation by Science and Technology doctoral fellowship.
[5] To whom correspondence should be addressed: Faculty of Science and Technology, Nanobiophysics, MIRA Institute for Biomedical Technology and Technical Medicine, University of Twente, Enschede (The Netherlands). Tel.: 31-0-534893655; Fax: 31-0-534891105; E-mail: k.broersen@utwente.nl.

[6] The abbreviations used are: AD, Alzheimer disease; SPR, surface plasmon resonance; HDX, hydrogen deuterium exchange; DMSO, dimethyl sulfoxide; TEM, transmission electron microscopy; ThT, thioflavin T; HSQC, heteronuclear single quantum coherence.

and $A\beta_{42}$. In the present study, we address how $A\beta_{40}$ and $A\beta_{42}$ influence and modulate assembly and consider how structural aspects of intermediates along the aggregation pathway can direct the cytotoxic response of $A\beta_{42}$:$A\beta_{40}$ ratios. By combining transmission electron microscopy (TEM), x-ray fiber diffraction, surface plasmon resonance (SPR), solution NMR, and high molecular weight mass spectrometry, we have characterized the start and end states of different relevant $A\beta_{42}$:$A\beta_{40}$ ratios. Using the unique combination of ^{15}N-edited and ^{15}N-filtered NMR experiments, we have been able to isolate the specific behavior of either $A\beta_{40}$ or $A\beta_{42}$ in mixtures. We show that $A\beta_{40}$ and $A\beta_{42}$ can interact and that they mutually influence their aggregation behavior. Interestingly, cross-seeding and mass spectrometry (MS) experiments reveal differences in the prefibrillar stage of aggregation, which are reflected by different aggregation kinetics.

EXPERIMENTAL PROCEDURES

Preparation of Aβ Peptide Ratios—The $A\beta_{40}$ and $A\beta_{42}$ peptides and their uniformly ^{15}N-labeled variants were purchased from rPeptide (rPeptide catalogue no. A-1153-1, A-1163-1, A-1101-2, and A-1102-2). The $A\beta_{40}$ and $A\beta_{42}$ peptides were combined in monomeric form in the desired ratios as described in detail elsewhere (28). In brief, Aβ peptides were dissolved in 1,1,1,3,3,3-hexafluor-2-propanol, $A\beta_{42}$ and $A\beta_{40}$ were then mixed in molar ratios of 1:9 and 3:7 together with pure $A\beta_{42}$ and $A\beta_{40}$ samples, and after evaporation of 1,1,1,3,3,3-hexafluor-2-propanol, they were redissolved in dimethyl sulfoxide (DMSO). The peptide was passed through a desalting column and eluted in a 50 mM Tris, 1 mM EDTA buffer, pH 7.5. Peptide concentrations were measured by the Bradford assay or by UV absorbance at 280 nm ($\epsilon_{280} = 1490\ \text{M}^{-1}\text{cm}^{-1}$). The samples were kept on ice until required, with a maximum lag time of 30 min.

SPR Analysis—N-terminally labeled biotin-linker chain $A\beta_{40}$ (biotin-$A\beta_{40}$) and biotin-$A\beta_{42}$ (rPeptide catalogue no. A-1112-1 and A-1118-1, respectively) and $A\beta_{40}$, $A\beta_{42}$, and a non-assembling peptide with the sequence KAAEAAAKKFFE (29) were treated as described above except using a 10 mM HEPES, 100 mM NaCl, 1 mM EDTA, and 0.05 mM NaN_3, pH 7.4 buffer, and the peptide was eluted using a 2-ml Zeba spin column for buffer exchange. SPR measurements were carried out on a Biacore® 2000 system (GE Healthcare) using carboxymethylated dextran preimmobilized with streptavidin sensor chips (GE Healthcare). A volume of 150 μl of biotin-$A\beta_{40}$ or biotin-$A\beta_{42}$ was immobilized to the sensor surface at a concentration of 10 μM at a flow rate of 30 μl/min. Concentrations of 10 μM of $A\beta_{40}$, $A\beta_{42}$ or KAAEAAAKKFFE were injected at 3 μl/min. Measurements were done in triplicate and analyzed with the built-in BIAevaluation software. Curve fitting relied on the Marquardt-Levenberg algorithm, and the change in response was fitted to the binding isotherm $R_{eq} = R_{max}[A]/((k_{off}/k_{on})+[A])$, where R_{eq} is the equilibrium response, R_{max} is the maximum signal response, [A] is the analyte concentration, k_{off} is the dissociation rate constant, and k_{on} is the association rate constant.

Fiber Diffraction—Samples of mature fibers were aligned by suspending a droplet of solution at 4 mg/ml between two wax-tipped capillaries positioned end-to-end. Fibers were mounted on a goniometer head, and x-ray diffraction data were collected using a Rigaku CuKα rotating anode with a wavelength of 1.5419 Å and RAxis IV++ detector. Specimen to detector distances were 160 and 250 mm with an exposure time of 10 min. Diffraction patterns were examined in CLEARER (30). For additional inspection, meridional, and equatorial axes signals were sampled through an angular search width of 60°, exported as a function of distance (pixels), and plotted using Braggs Law.

TEM Analysis—Aliquots of 4 μl Aβ were adsorbed for 30 s onto freshly prepared carbon-coated and glow-discharged copper grids, washed briefly with milli-Q water, and subsequently stained with 1% (*w/v*) uranyl acetate for 30 s. Samples were examined with a JEOL 1200 transmission electron microscope operating at 100 KV.

Cross-seeding Monitored with ThT—Aliquots (100 μl) of each Aβ ratio at 50 μM were incubated at 25 °C in 50 mM Tris, 1 mM EDTA, pH 7.5. After 24 h incubation these samples were sonicated at 4 °C for 10 min at maximum power and mixed with freshly and simultaneously prepared Aβ ratios to induce (cross-)seeding of Aβ aggregation. Final concentrations in these mixtures were 0.5 μM of sonicated Aβ and 25 μM of monomeric Aβ. The seed preparations were examined by TEM.

ThT Fluorescence—Aβ peptide samples of 25 μM were incubated with 12 μM thioflavin T (ThT) in a total volume of 150 μl in a Greiner 96-well plate. Fibrillization kinetics were followed using a Fluostar OPTIMA fluorescence plate reader using 440 nm excitation wavelength and an emission wavelength of 480 nm. Readings were recorded in triplicate every 10 min for a period of 24 h.

High Molecular Weight MS—High mass measurements were performed at CovalX AG (Schlieren, Switzerland) using an ABI 4800 MALDI TOF mass spectrometer retrofitted with CovalX HM2 TUVO high mass system. A phosphate-buffered saline buffer was used to prepare the Aβ ratios, which were subjected to cross-linking with gluteraldehyde at specific time points. Each sample was mixed with sinapinic acid matrix (10 mg/ml) in acetonitrile/water (1:1, *v/v*), TFA 0.1% and spotted on the MALDI plate (SCOUT 384, AchorChip). High-mass MALDI TOF MS analysis was performed using standard nitrogen laser and focusing on different mass ranges from 8 to 1000 kDa in linear and positive mode and at a gain voltage of 3.14 kV and an acceleration voltage of 20 kV for HM2 High-Mass detection. The instrument was calibrated using insulin, BSA, and IgG. The analysis was repeated in triplicate.

Solution NMR—Aβ samples for NMR studies varied between 20 and 200 μM (monomer concentration) in 50 mM Tris-HCl, 1 mM EDTA at pH 7.5, supplemented with 10% (*v/v*) D_2O (>99.96%, Sigma Aldrich). The experiments were performed at 25 °C either on a Bruker Avance (equipped with cryoprobe) or on a Varian Inova spectrometer both operating at 14.1 Teslas (600 MHz). ^{15}N sofast heteronuclear single quantum coherence (HSQC) spectra were each collected over 30 min to monitor aggregation. ^{15}N NOESY-HSQC and ^{1}H,^{1}H TOCSY experiments were recorded at 5 °C to obtain sequence specific $^{1}H_N$,^{15}N assignments to identify the HSQC peaks. A combination of ^{15}N-edited and ^{15}N-filtered experiments (31) acquired on samples containing uniformly ^{15}N-labeled and unlabeled

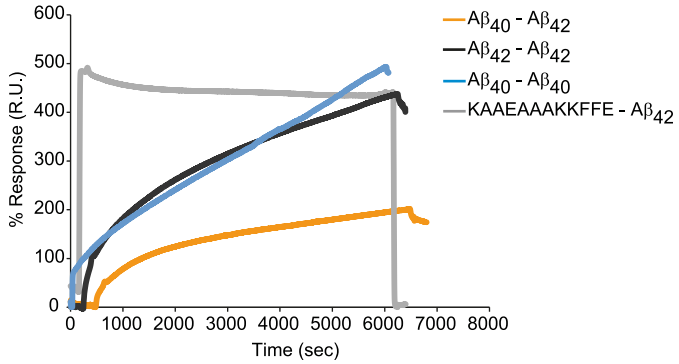

FIGURE 1. **$A\beta_{40}$ and $A\beta_{42}$ interact directly.** 10 μM covalently tethered biotinylated $A\beta_{40}$ or $A\beta_{42}$ to streptavidin-coated SA chips show binding between 10 μM Aβ variants. The sensorgram presents the interaction between $A\beta_{40}$-$A\beta_{42}$ (*orange*), $A\beta_{42}$-$A\beta_{42}$ (*black*), $A\beta_{40}$-$A\beta_{40}$ (*blue*), and the negative control nonspecific binding between $A\beta_{42}$-KAAEAAAKKFFE (*gray*).

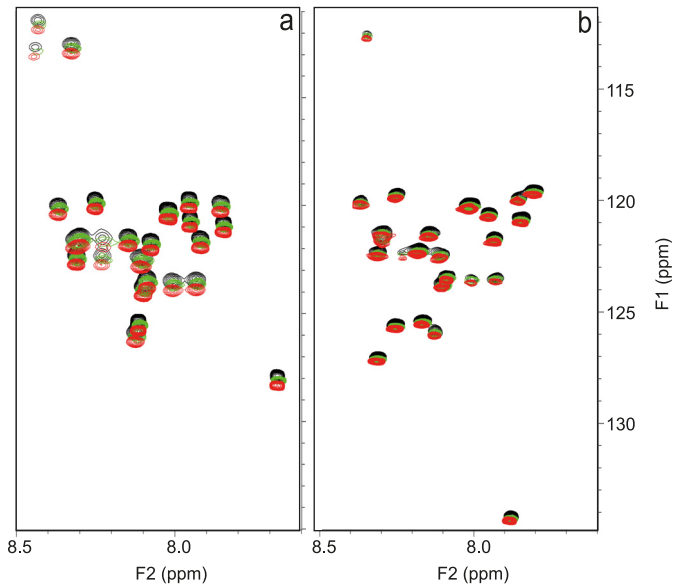

FIGURE 2. **The monomeric structures of $A\beta_{42}$:$A\beta_{40}$ ratios are identical at atomic level.** Shown is the overlay of the ^{1}H-^{15}N HSQC spectra immediately after sample preparation of *a*, ^{15}N-labeled $A\beta_{40}$ in pure $A\beta_{40}$ sample (*black*), ratio $1{:}9_{(15\ N)}$ (*green*) and ratio $3{:}7_{(15\ N)}$ (*red*). *b*, ^{15}N-labeled $A\beta_{42}$ in pure $A\beta_{42}$ sample (*black*), ratio $1_{(15\ N)}$:9 (*red*), and ratio $3_{(15\ N)}$:7 (*green*). For representation purposes and clarity, we have artificially introduced a systematic shift of the spectra of the 1:9 and 3:7 $A\beta_{42}$:$A\beta_{40}$ ratios.

Aβ peptides at different ratios was used to selectively monitor $A\beta_{42}$ and $A\beta_{40}$ in solution.

Protection factors of mature Aβ fibers were measured by comparing the amide peak intensities obtained for Aβ samples incubated in H_2O or in D_2O after for a period of 672 h to allow amide exchange. The fibers were collected by centrifugation, washed, and incubated in D_2O at 25 °C for 48 h, flash-frozen to quench the hydrogen-deuterium exchange (HDX), lyophilized, and redissolved in 100% DMSO-d_6 (99.9%, Cambridge Isotope Laboratories) acidified with 0.1% (*v/v*) trifluoroacetic acid (Fluka) for 30 s, followed by a 10-fold dilution with perdeuterated DMSO (32). Amide exchange was measured by collecting two-dimensional ^{15}N-^{1}H HSQC spectra in comparison to control samples that were incubated in H_2O. The ^{15}N-^{1}H HSQC cross-peak assignment was confirmed with a ^{15}N-resolved NOESY experiment.

Cross-seeding Monitored via NMR—Seeds were prepared of pure $A\beta_{40}$ or pure $A\beta_{42}$ as described above. An aliquot of 30 μl seeds (50 μM equivalent monomeric concentration) was mixed with 330 μl of the corresponding Aβ samples that were preincubated in an NMR tube (Shigemi), whereas the non-seeded signals were monitored. ^{15}N-edited and ^{15}N-filtered spectra (31) were acquired as a function of time to simultaneously monitor both Aβ alloforms in the 1:9 and 3:7 ratios, whereby $A\beta_{42}$ was ^{15}N-labeled and $A\beta_{40}$ was unlabeled. Only one-dimensional proton spectra were recorded as a function of time for the pure $A\beta_{40}$ or pure $A\beta_{42}$ unlabeled samples.

RESULTS

Direct Interactions between $A\beta_{40}$ and $A\beta_{42}$—SPR was used to explore whether $A\beta_{40}$ and $A\beta_{42}$ are able to directly associate. Either biotinylated $A\beta_{42}$ or $A\beta_{40}$ were tethered to a chip and measurements of interactions between $A\beta_{42}$-$A\beta_{42}$ and $A\beta_{40}$-$A\beta_{40}$ adsorption resulted in initial fast adsorption of the Aβ peptides, followed by a slower kinetics phase of peptide binding, characteristic for high affinity binding (Fig. 1). A similar binding profile has been reported for the aggregation and fibrillization of isolated $A\beta_{42}$, where a high incidence of specific binding is observed between 11-mercaptoundecanoic acid tethered $A\beta_{42}$ and monomeric $A\beta_{42}$ in bulk solution (33). The interaction between tethered $A\beta_{42}$ with $A\beta_{40}$ monomers showed a similar binding profile but slightly weaker binding. Binding between the same Aβ alloform resulted in greater mass adsorption to the sensor surface compared with mixed Aβ oligomeric interactions. These data show that the strongest binding occurs between the same alloform such as $A\beta_{42}$-$A\beta_{42}$ or $A\beta_{40}$-$A\beta_{40}$. However, strong specific binding was also observed between $A\beta_{42}$-$A\beta_{40}$.

Different Molar $A\beta_{42}$:$A\beta_{40}$ Ratios Are Structurally Similar at Beginning of Aggregation Process—Because $A\beta_{42}$ and $A\beta_{40}$ were found to interact directly, we used NMR to explore whether the interactions could influence the conformation of Aβ at different $A\beta_{42}$:$A\beta_{40}$ ratios immediately following their preparation. The peptides were treated according to a new protocol designed to yield completely solubilized samples without solvent contamination (13). ^{15}N-labeling of one Aβ alloform at a time allowed us to monitor the individual structural behavior of each alloform within the context of different molar ratios. The structural fingerprints of pure $A\beta_{42}$ and $A\beta_{40}$ peptides by the ^{15}N-$^{1}H_N$ HSQC spectra are in excellent agreement with data shown in the literature (Fig. 2) (27, 34). The spectra of ^{15}N-labeled $A\beta_{42}$ at different molar ratios do not present chemical shift variations, not even for the resonances of the C terminus, which should be the most sensitive to even a small change of environment (Fig. 2*B*). This indicates that the co-presence of the two alloforms has no influence on the structure at an atomic level, as expected for the monomeric state. The same is observed for $A\beta_{40}$ (Fig. 2*A*). We conclude that samples with different Aβ ratios are structurally equivalent to samples of pure individual peptides prior to aggregation.

Fibers Formed by Different Aβ Ratios Have Similar Morphology and Cross-β Structure—Negative stain TEM was used for a morphological characterization of the end states of the Aβ aggregation reactions. Upon long term incubation, all Aβ

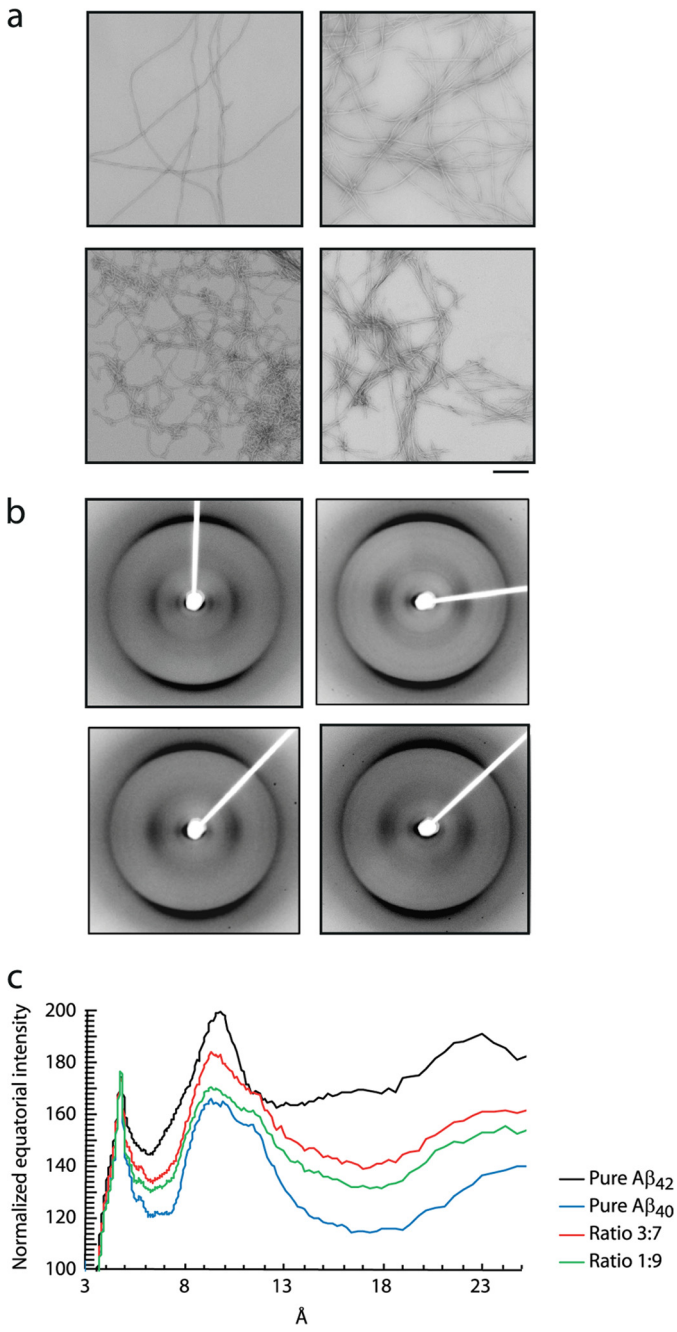

FIGURE 3. **Morphology and detailed structure analysis of fibrils of Aβ42:Aβ40 ratios reveals similar structural characteristics.** *a*, TEM images of Aβ ratios obtained upon aggregation for 2 weeks at 25 °C without agitation. *Top left panel*, pure $A\beta_{40}$; *top right panel*, ratio 1:9; *bottom left panel*, ratio 3:7; *bottom right panel*, pure $A\beta_{42}$. *Bar*, 200 nm. *b*, fiber diffraction patterns of Aβ ratios obtained upon aggregation for 4 weeks at 25 °C without agitation. *Top left panel*, pure $A\beta_{40}$; *top right panel*, ratio 1:9; *bottom left panel*, ratio 3:7; *bottom right panel*, pure $A\beta_{42}$. *c*, overlay showing the normalized x-ray scattering intensity function of D-spacing plotted from *b*.

ratios display a similar morphology with long, unbranched amyloid fibrils with detectable helicity and uniform diameters of 5.4, 10.2, and 16 nm, depending on the number of laterally associated protofilaments (Fig. 3*A*). At a qualitative level, the fibrillar structure of the 3:7 ratio of $A\beta_{42}$:$A\beta_{40}$ appeared to be slightly more polymorphic compared with the other ratios.

X-ray fiber diffraction showed that the samples of pure Aβ and mixed ratios all exhibit the classic cross-β fiber diffraction patterns described in the literature (38, 39), showing a strong meridional reflection at 4.7 Å and a major equatorial reflection at ~10 Å consistent with a cross-β architecture (Fig. 3*B*). The patterns arising from $A\beta_{42}$ and $A\beta_{40}$ fibrils both share the same 9.7–9.8 Å major equatorial reflection, which we attribute to the β-sheet spacing perpendicular to the fiber axis. The fiber diffraction pattern obtained from $A\beta_{42}$ fibrils was distinguishable from $A\beta_{40}$ fibrils only by the sharper signals likely to arise from a higher degree of order in the $A\beta_{42}$ fibers, whereas the mixtures of the two peptides give rise to patterns that are virtually indistinguishable from that of $A\beta_{40}$. This could be due to the large amount of $A\beta_{40}$ relative to $A\beta_{42}$ such that the signal from $A\beta_{40}$ dominates the pattern. Although subtle differences in the fiber diffraction patterns likely arise from differing degrees of order and composition of the samples, the equatorial signal positions and relative intensities of signals are largely comparable for all samples (Fig. 3*C*).

To confirm structural similarity of fiber architecture of various Aβ ratios at a higher resolution, we measured the protection factors of the Aβ peptides by acquiring ^{15}N-$^{1}H_N$ HSQC spectra for monomeric $A\beta_{40}$ and $A\beta_{42}$ after resolubilizing amyloid fibers that were subjected to HDX (supplemental Fig. S1). Amide protection factors were measured by comparing the amide peak intensities obtained for the sample in H_2O and the sample in D_2O after the exchange period. The backbone amide chemical shift data are consistent with those previously reported in acidified DMSO-d_6 (32), although we observed (partial) overlaps in the cross-peaks of residues 11/23, 12/18, 13/27, 19/40, and 32/41 for $A\beta_{42}$ (supplemental data). Only residues 11/23 and 13/27 have overlapping cross-peaks in the $A\beta_{40}$ spectrum. The HDX pattern of ^{15}N-labeled $A\beta_{40}$ for the $1{:}9_{(15\ N)}$ and $3{:}7_{(15\ N)}$ ratios and for pure $A\beta_{40}$ fibers shows that the stretches comprising residues 18–22 and 30–34 are more protected from solvent exchange than the N terminus (supplemental Fig. S2). The C-terminal residues 37–40 also appear more accessible to solvent exchange. This agrees with earlier observations and proposed models for $A\beta_{40}$ fibrils (18, 40–42). The HDX patterns of ^{15}N-labeled $A\beta_{42}$, $A\beta_{40}$, and the ratios showed only small differences. Extensive exchange times (up to 672 h) (supplemental Fig. S2) of $A\beta_{42}$ showed no noticeable effects in agreement with the suggestion that $A\beta_{42}$ fibrils are highly resistant to solvent exchange (32, 43). The pattern for pure $A\beta_{42}$ and the $3_{(15\ N)}$:7 and $1_{(15\ N)}$:9 ratios is less distinct but indicates a clear distinction between the N- and the C-terminal halves with higher protection of the C-terminal half.

We conclude that the architecture of Aβ fibers in pure or mixed form is overall indistinguishable both at a macromolecular and high resolution level, although small differences at atomic level may be present. As these mature fibrils have been shown to have weak toxicity, we will focus on differences in the oligomeric regime.

$A\beta_{40}$ and $A\beta_{42}$ Affect Aggregation Kinetics of the Other—To address whether aggregation kinetics are affected by different ratios, we monitored the intensity of NMR spectra as a function of time, exploiting the disappearance of the resonances due to the increased molecular weight, typical of events in a slow

exchange regime. We exploited again the possibility of ^{15}N-isotope labeling only one of the Aβ alloforms, in combination with ^{15}N-edited filter experiments to monitor the aggregation of both the ^{15}N-labeled and unlabeled peptides simultaneously. This experimental setup offers the advantage that the individual Aβ alloforms are selectively observed in parallel and within the same sample preparation, thereby circumventing any uncertainty that might arise from different sample preparations or peptide batches. In all cases, we observed the concomitant disappearance of all peaks according to a cooperative behavior along the whole peptide or at least the region of it visible in the NMR spectrum. No sufficiently populated lower molecular weight assemblies were observed, indicating that Aβ aggregates directly into NMR invisible assemblies under these experimental conditions. Due to the long apparent lag phase, we did not detect a sigmoidal transition for $A\beta_{40}$ and the 1:9 ratio over a time scale of 180 h (Fig. 4, *A*, *E*, and *F*). In contrast, pure $A\beta_{42}$ aggregates very rapidly with a sigmoidal signal disappearance (Fig. 4*B*). Interestingly, the $A\beta_{42}$ component of the 1:9 ratio remains in solution significantly longer in the presence of $A\beta_{40}$. The kinetics recorded for $A\beta_{40}$ and $A\beta_{42}$ within the 3:7 ratios with either ^{15}N-labeled $A\beta_{42}$ or ^{15}N-labeled $A\beta_{40}$ (named $3_{(15\ N)}$:7 and $3:7_{(15\ N)}$, respectively) indicate that $A\beta_{40}$ remains longer in solution compared with $A\beta_{42}$, which aggregates more rapidly (Fig. 4, *C* and *D*). However, the complete loss of signal for $A\beta_{42}$ in the presence of $A\beta_{40}$ is delayed in comparison with pure $A\beta_{42}$, suggesting that the shorter $A\beta_{40}$ alloform reduces the aggregation propensity of the longer $A\beta_{42}$ alloform. To make sure that these observations could not be explained as the average of populations containing only the same alloforms, we analyzed a 5:5 ratio where ^{15}N-labeled $A\beta_{42}$ or $A\beta_{40}$ are present in equimolar amounts of the unlabeled alloform (Fig. 4, *G* and *H*). We observed a nearly simultaneous disappearance of the signals of $A\beta_{42}$ and $A\beta_{40}$, which strongly suggests co-aggregation of both peptides into mixed fibers. We conclude that $A\beta_{40}$ and $A\beta_{42}$ mutually influence the aggregation kinetics of the other.

$A\beta_{40}$ and $A\beta_{42}$ Ratios Both Form Complex but Different Ensembles of Oligomers—To investigate whether the observed alloform influence on the aggregation arises from an impact on the formation of intermediates along the aggregation pathway, we followed aggregation of the Aβ mixtures using high molecular weight MS, a technique that uses high voltages to enable detection of high molecular weight species. Because non-covalent complexes disassemble at these voltages, we incubated our samples prior to analysis with glutaraldehyde as cross-linking agent. The resulting masses reveal various interesting features (Fig. 5 and supplemental Table S1). First, the masses of $A\beta_{42}$ and of the two mixtures are consistently larger than those of $A\beta_{40}$, in support of the hypothesis that there are appreciable populations of oligomers that contain both alloforms. Second, early aggregation proceeds through a monomer addition process during which oligomers gradually grow by the addition of one monomer at a time. Third, in all cases we observed that assemblies accumulate during aggregation, the maximum size of which depends on the $A\beta_{42}$:$A\beta_{40}$ ratio. At an incubation time of 1 h, $A\beta_{40}$ samples contain oligomers with a range of sizes from dimers up to 13-mers. As the process continues, larger oligomers are formed and after 6 h of incubation, 25-mer assemblies are detected together with larger oligomers at apparent molecular weights of 186 up to 852 kDa. For 1:9 ratios, we observe formation of much smaller oligomers with a maximum of 8-mers and accumulation of larger sized oligomers at apparent molecular masses of 171 up to 515 kDa. The 3:7 ratios aggregate in a similar manner but share features closer to the pattern observed for $A\beta_{42}$. No very large molecular weight oligomers are observed after 6 h of incubation, presumably because they become so large that either they cannot become mobile or are not efficiently cross-linked. These results reveal clear differences in the pattern of small oligomeric species formed under different ratio conditions, indicating a potential basis for the difference in toxic effect (13).

Differences between $A\beta_{42}$:$A\beta_{40}$ Ratios Reside along Aggregation Pathway—The influence of the $A\beta_{40}$ and $A\beta_{42}$ ratios on aggregation kinetics is also evident from cross-seeding experiments where sonicated protofibrils were added to monomeric solutions of different $A\beta_{42}$:$A\beta_{40}$ ratios. Seed preparations were verified by TEM (Fig. 6*A*) and added to freshly prepared monomeric Aβ solutions. The aggregation kinetics were followed by *in situ* ThT fluorescence (Fig. 6, *B–E*). $A\beta_{40}$ aggregation was efficiently seeded by $A\beta_{40}$ seeds and the 1:9 ratio seeds leading to elimination of the lag phase (Fig. 6*B*). The initial parts of the two curves overlap, indicating that the properties of $A\beta_{40}$ are predominant, also in the 1:9 mixture. Addition of 3:7 seeds also induces aggregation, but some lag phase is retained. Addition of pure $A\beta_{42}$ not only does not seed aggregation, but even lengthens the lag phase. Seeding of $A\beta_{40}$ therefore appears to proceed in a highly specific manner with preference for the same alloform seeds. The 1:9 ratio is seeded by any seed but, as for pure $A\beta_{40}$, $A\beta_{40}$, and 1:9 seeds have a similar strong seeding effect, whereas $A\beta_{42}$ and 3:7 seeds have a milder effect, which, however, still preferentially selects the same alloform (Fig. 6*C*). In contrast, pure $A\beta_{42}$ and the 3:7 ratio were equally effectively seeded by any Aβ seed, regardless of whether they were formed from $A\beta_{40}$ or $A\beta_{42}$ or a mixture (Fig. 6, *D* and *E*). Therefore, it appears that $A\beta_{42}$ monomers have a higher degree of plasticity so that they may use a less specific surface as a template, whereas $A\beta_{40}$ oligomers have higher selectivity.

The effect of cross-seeding on the disappearance of the NMR signals of the different Aβ alloforms was also studied. In these experiments, we limited ourselves to the addition of seeds of pure $A\beta_{40}$ or pure $A\beta_{42}$ to the preincubated samples of which the NMR signals were monitored. In all cases, adding seeds resulted in appreciable aggregation irrespectively of the time point at which the addition was made. The control experiments were performed without any addition and this ensured that the effect is the direct consequence of the addition. Pure $A\beta_{42}$ monomers could be easily seeded by both peptides (Figs. 7, *C* and *D*). Induction of aggregation of $A\beta_{40}$ with $A\beta_{40}$ seeds was also highly efficient (Fig. 7*B*), whereas $A\beta_{42}$ seeds induced some initial signal disappearance but with a delayed aggregation (Fig. 7*A*). In the 1:9 and 3:7 ratios, $A\beta_{40}$ seeds could efficiently induce aggregation of the two Aβ alloforms in the mixtures, while the $A\beta_{42}$ seeds efficiently seeded the $A\beta_{42}$ alloform, whereas the $A\beta_{40}$ alloform lags behind in the aggregation. This implies that the presence of $A\beta_{42}$ monomers in the ratios influences the behavior of the $A\beta_{40}$ alloform. Overall, it is observed that the $A\beta_{40}$ seeds can efficiently induce aggregation of

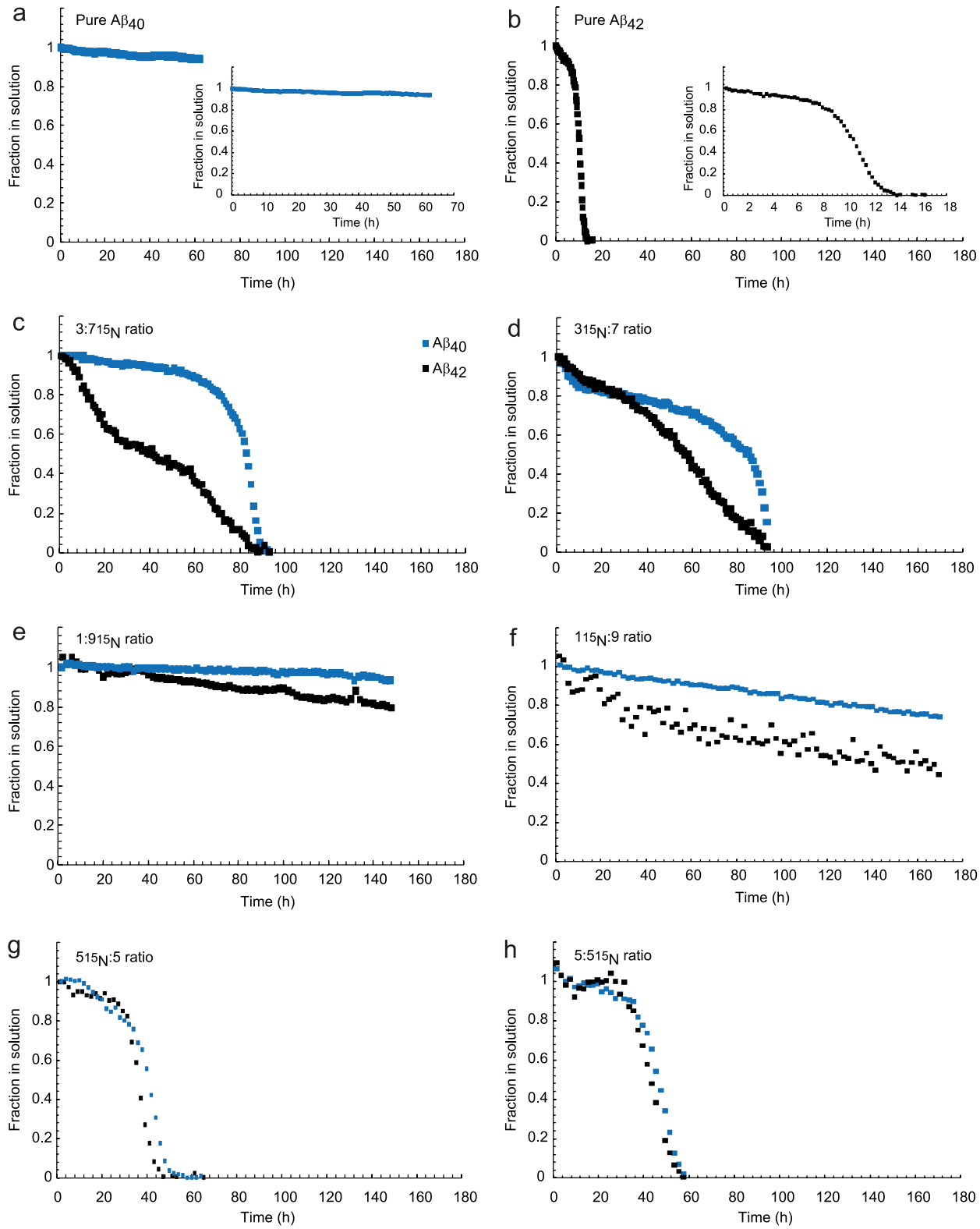

FIGURE 4. **Aβ$_{40}$ and Aβ$_{42}$ show different aggregation behavior in different Aβ$_{42}$:Aβ$_{40}$ ratios.** *a*, pure Aβ$_{40}$ at a concentration of 180 μM does not aggregate within the timeframe of data collection. *b*, pure Aβ$_{42}$ at a concentration of 20 μM displays a lag phase and a sigmoidal transition from monomeric species into NMR invisible aggregates. *c*, 3:7$_{(15\ N)}$ ratio, whereby the Aβ sample is composed of 70% ^{15}N-labeled Aβ$_{40}$, which is monitored via HSQC (140 μM Aβ$_{40}$ monomer concentration) and 30% unlabeled Aβ$_{42}$ (at a monomer concentration of 60 μM), which is simultaneously monitored via the amide region ^{15}N-filtered one-dimensional NMR spectrum. *d*, the 3$_{(15\ N)}$:7 ratio whereby the Aβ sample is composed of 30% ^{15}N-labeled Aβ$_{42}$ and 70% unlabeled Aβ$_{40}$. *e*, the 1:9$_{(15\ N)}$ ratio with 10% unlabeled Aβ$_{42}$ (20 μM) and 90% ^{15}N-labeled Aβ$_{40}$ (180 μM). *f*, the 1$_{(15\ N)}$:9 ratio with 10% ^{15}N-labeled Aβ$_{42}$ and 90% unlabeled Aβ$_{40}$. *g*, the 5$_{(15\ N)}$:5 ratio whereby the ^{15}N-labeled Aβ$_{42}$ and unlabeled Aβ$_{40}$ are present in equimolar amounts (60 μM of each alloform). *h*, the 5:5$_{(15\ N)}$ ratio whereby equimolar amounts (60 μM) of unlabeled Aβ$_{42}$ and ^{15}N-labeled Aβ$_{40}$ are present. The *blue symbols* represent Aβ$_{40}$, and the *black symbols* correspond to Aβ$_{42}$.

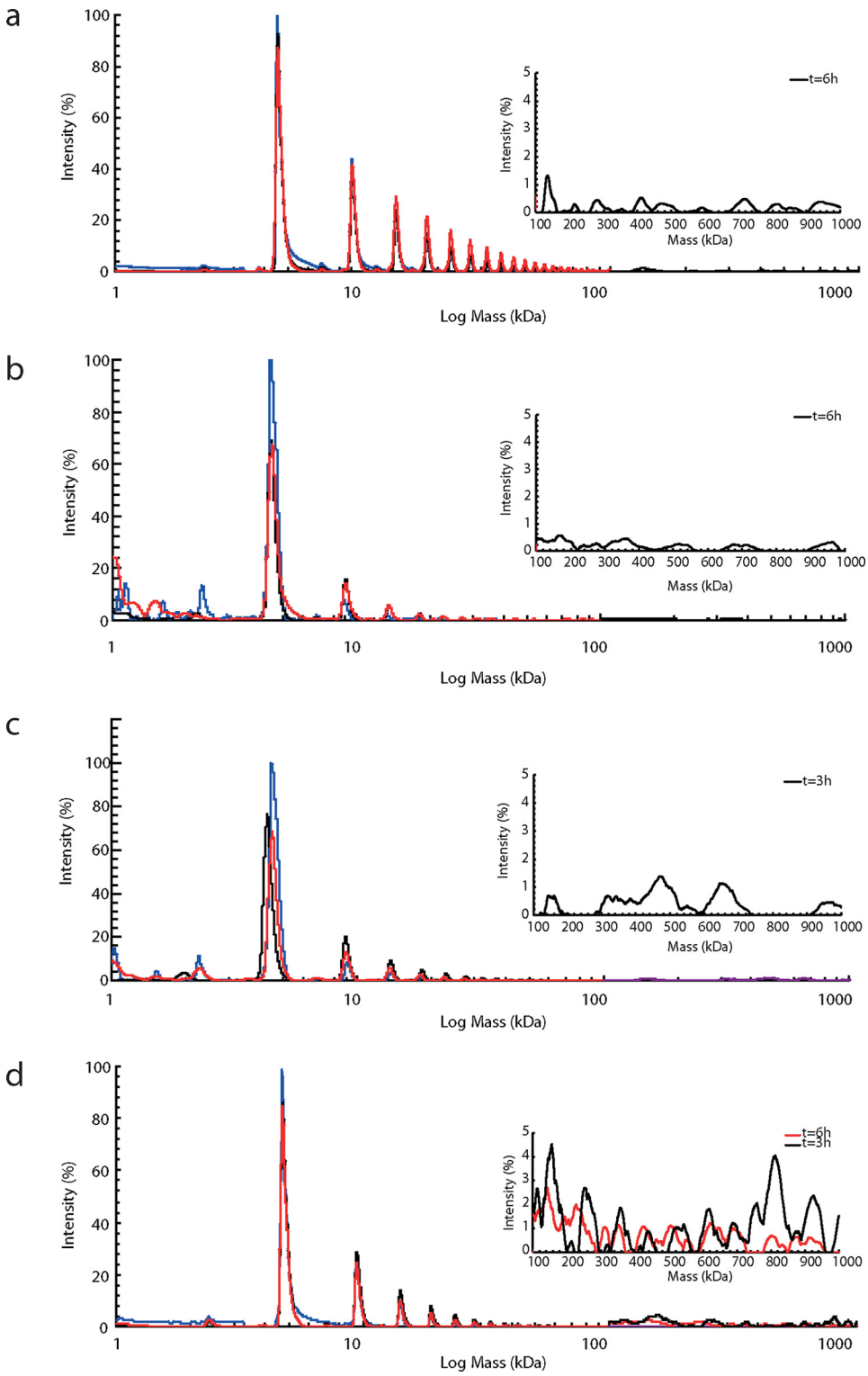

FIGURE 5. **Oligomer formation by Aβ$_{42}$:Aβ$_{40}$ ratios shows a monomer addition process and a dynamic distribution of oligomeric species.** Mass spectra of the different ratios with the high molecular weight detection spectra as *insets* whereby the *blue trace* is $t = 1$ h, the *black trace* is $t = 3$ h, and the *red trace* is $t = 6$ h. *a*, pure Aβ$_{40}$; *b*, 1:9 ratio; *c*, 3:7 ratio; *d*, pure Aβ$_{42}$. These aggregation patterns for the different ratios are also presented in supplemental Table S1.

Aβ samples, whereas the Aβ$_{40}$ alloform responds less efficiently to the Aβ$_{42}$ seeds (Fig. 8 and Table 1). These data show a genuine difference between the two peptides at the level of the oligomeric state. They reveal that even a relatively small increase in Aβ$_{42}$ in the mixture confers aggregation properties to Aβ$_{40}$ that are markedly more similar to pure Aβ$_{42}$.

DISCUSSION

Although previous structural studies have mostly focused on pure Aβ alloforms and the identification of a single oligomeric species, the present work aims to understand the determinants of the toxicity of different Aβ$_{42}$:Aβ$_{40}$ ratios. We demonstrate by

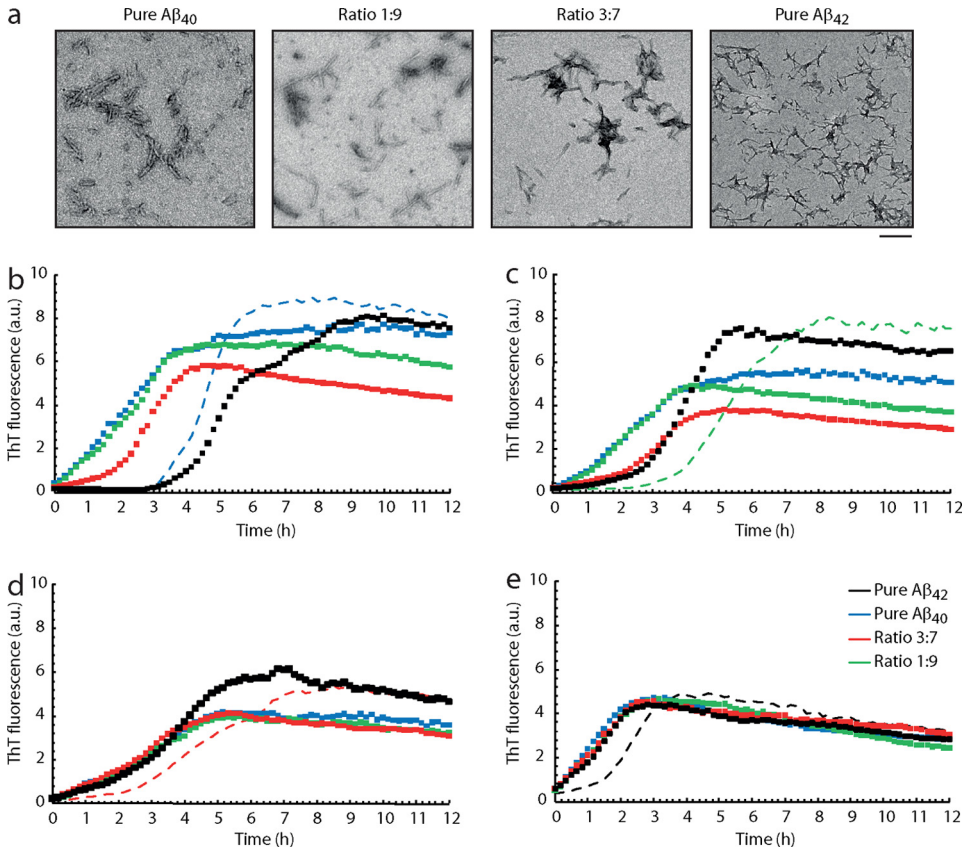

FIGURE 6. **Cross-seeding reveals that Aβ$_{42}$ oligomers show plasticity, whereas Aβ$_{40}$ oligomers display a higher selectivity.** *a*, TEM of seed preparations. Seeds were prepared by incubation of 50 μM Aβ ratios for 24 h followed by sonication at maximum power for 10 min. From *left* to *right*: pure Aβ$_{40}$, ratio 1:9; ratio 3:7, pure Aβ$_{42}$. *Bar*, 0.2 μm. Freshly prepared seeds were added to monomeric solutions of Aβ$_{42}$:Aβ$_{40}$ ratios at final concentrations of 0.5 μM and 25 μM, respectively. *b*, ThT of Aβ$_{40}$ monomers seeded with pure Aβ$_{40}$ seeds (*blue dotted trace*); with seeds from ratio 1:9 (*green dotted trace*), with seeds from ratio 3:7 (*red dotted trace*), and with seeds from pure Aβ$_{42}$ (*black dotted trace*). The *blue dashed line* represents the unseeded Aβ$_{40}$ control. *c*, ThT of ratio 1:9 monomers seeded with Aβ ratios as compared with the non-seeded aggregation curve. The colors are as described in *b*. *d*, ThT of ratio 3:7 monomers seeded with Aβ ratios as compared with the non-seeded aggregation curve (*red dashed line*). Colors are as described in *b*. *e*, ThT of Aβ$_{42}$ monomers seeded with Aβ ratios in comparison with the non-seeded sample (*black dashed line*). Colors are as described in *b*.

independent evidence from MS, NMR, and SPR that the two peptides interact, although recognition between the same alloforms is preferred over interactions between different ones. We therefore expect that the populations of the two peptides in the aggregates will be mixed. This explains and expands previous data (23, 25, 27) that indicate that Aβ$_{40}$ and Aβ$_{42}$ influence their respective aggregation properties.

To understand which step along the aggregation pathway is responsible for this effect, we compared the structures and morphologies of all the species formed. We show that the initial monomeric and final fibrillar states do not differ to a large extent. NMR analysis of freshly prepared samples at different Aβ$_{42}$:Aβ$_{40}$ ratios conclusively reveals the presence of predominant monomeric species that lack a regular and well defined structure. Therefore, at this stage, the peptides are not affected by the presence of the other alloform. Likewise, we do not observe appreciable differences between the mature fibrillar states by TEM, HDX, and fiber diffraction: fibers formed during long incubation times are virtually identical. The absence of significant differences in the start and end points of Aβ fibrillation directed our focus to the formation of transient oligomeric intermediates. Previous data had indicated differences in the protofibrillar morphologies and Fourier transform infrared spectroscopy data following short term incubation, which, together with the present data, underline the importance of the aggregation pathway and of the dynamics of the oligomeric state (13, 44, 45).

We observed subtle but clear differences between the different Aβ ratios along the aggregation pathway. NMR experiments visualizing the spontaneous aggregation (Fig. 4) showed that the presence of monomeric Aβ$_{40}$ slows down the aggregation kinetics of Aβ$_{42}$, increasing the time frame that soluble forms are found in solution for any peptide ratio. *Vice versa* Aβ$_{42}$ stimulates Aβ$_{40}$ aggregation as revealed by comparing the 3:7 and 1:9 ratios with pure Aβ$_{40}$. This is compatible with the view that Aβ$_{42}$ drives aggregation and acts as a template by lowering the kinetic barriers that prevent Aβ$_{40}$ from aggregating (15, 25, 46). Aβ$_{40}$ potentially delays Aβ$_{42}$ aggregation through "non-productive" interactions. Although these conclusions are in agreement with previous reports (25, 27, 46), our cross-seeding data suggest that Aβ$_{40}$ monomers specifically require Aβ$_{40}$ oligomers to induce growth of mature fibrils, whereas Aβ$_{42}$ monomers are less selective and are stimulated by all types of seeds.

It might be argued that there is an apparent discrepancy between the progressive Aβ aggregation as monitored by NMR (Fig. 4) and the cross-seeding data (Figs. 6–8). By NMR, we observe that Aβ$_{42}$ stimulates Aβ$_{40}$ to aggregate while Aβ$_{40}$

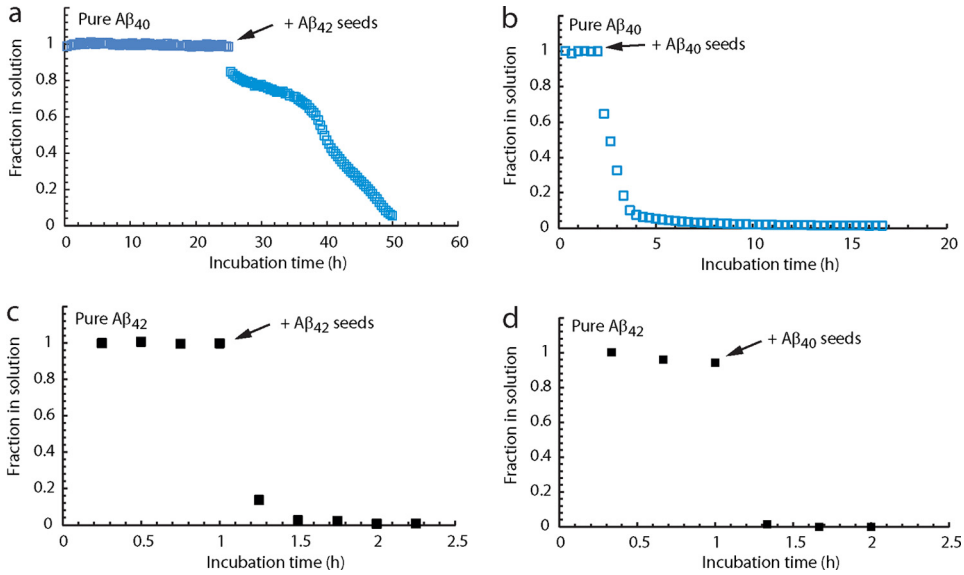

FIGURE 7. **Cross-seeding was monitored by NMR by recording one-dimensional proton spectra as a function of time with unlabeled pure Aβ$_{40}$ (*a* and *b*) and pure Aβ$_{42}$ (*c* and *d*) monomers using preformed Aβ$_{40}$ seeds (*b* and *d*) and Aβ$_{42}$ seeds (*a* and *c*).** Pure Aβ$_{40}$ samples (*blue*) were prepared at a concentration of 180 μM, whereas pure Aβ$_{42}$ samples (*black*) were at a concentration of 20 μM. The addition of 10% (*v/v*) of a 50 μM (monomeric equivalent) seed preparation was added at the time points indicated by the *arrow*.

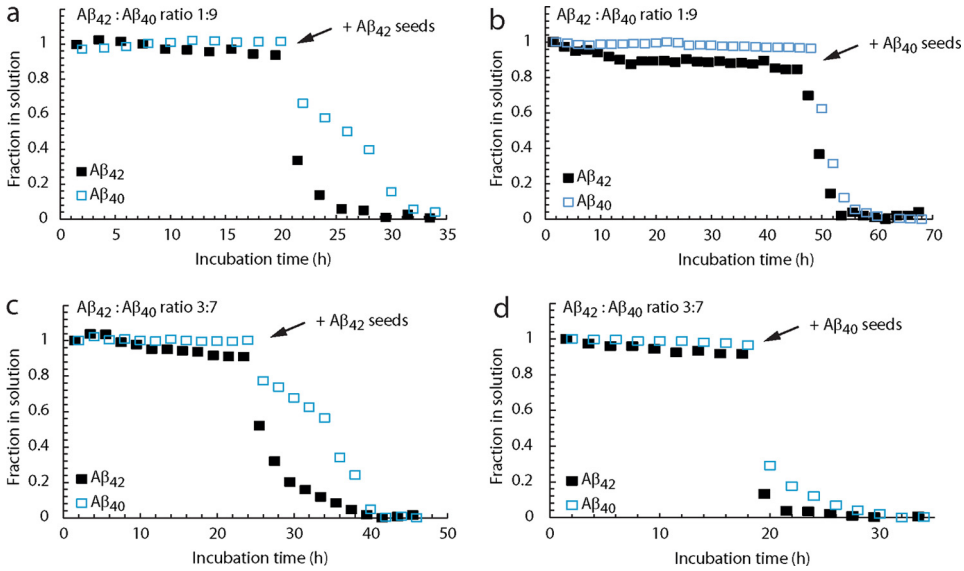

FIGURE 8. **Cross-seeding was monitored by ^{15}N-filtered and ^{15}N-edited NMR experiments with Aβ samples composed of the Aβ$_{42}$:Aβ$_{40}$ ratio 1$_{(15\ N)}$:9 (*a* and *b*), whereby 20 μM ^{15}N-labeled Aβ$_{42}$ is present with 180 μM unlabeled Aβ$_{40}$ and the Aβ$_{42}$:Aβ$_{40}$ ratio 3$_{(15\ N)}$:7 (*c* and *d*) with 60 μM ^{15}N-labeled Aβ$_{42}$ and 140 μM unlabeled Aβ$_{40}$.** The addition of 10% (*v/v*) of a 50 μM (monomeric equivalent) preparation of preformed Aβ$_{40}$ seeds (*b* and *d*) and Aβ$_{42}$ seeds (*a* and *c*) is indicated by the *arrows*.

simultaneously delays Aβ$_{42}$ aggregation. *Vice versa*, the cross-seeding data reveal that monomeric Aβ$_{40}$ is not efficiently seeded by sonicated Aβ$_{42}$ protofibrils. It is reasonable to explain this discrepancy by assuming that the oligomers formed during the aggregation process have features that are distinct from the sonicated protofibrillar species (seeds) that may have undergone advanced structural maturation. For pure Aβ$_{42}$, these seeds would not be the optimal templates to directly incorporate Aβ$_{40}$ monomers and perhaps even entail a conformational restructuring to lead to productive aggregation. We cannot rule out the possibility that monomeric Aβ$_{40}$ could be able to resolubilize Aβ$_{42}$ seeds, thereby bringing Aβ$_{42}$ into solution and promoting in this way productive aggregation, as hinted by Yan and Wang (27). Because our observations with high molecular weight MS underline that the aggregation process proceeds through a monomer addition mechanism, the dynamic interplay (productive and non-productive) of monomeric Aβ with soluble Aβ assemblies seems appropriate to explain toxicity of the Aβ$_{42}$:Aβ$_{40}$ ratios. This relevance of monomer addition processes for neurotoxicity was recently described by Jan and colleagues for pure Aβ$_{42}$ aggregation (44). Thus, the modulation of the Aβ oligomer formation by the Aβ$_{42}$:Aβ$_{40}$ ratio adds to the cause of neurotoxicity and the Alzheimer disease pathology.

In conclusion, our work indicates that the Aβ$_{42}$:Aβ$_{40}$ ratio behavior cannot be simply interpreted by stating that Aβ$_{42}$ can

TABLE 1
Efficiency of cross-seeding on Aβ alloforms as monitored by isotope-labeled NMR

		Efficiency of seeding monitored by NMR	
Monomeric sample	**Seeds**	**$A\beta_{42}$**	**$A\beta_{40}$**
Pure $A\beta_{42}$	$A\beta_{40}$	+++	NA[a]
	$A\beta_{42}$	+++	NA
$A\beta_{42}$:$A\beta_{40}$ ratio 3:7	$A\beta_{40}$	+++	+++
	$A\beta_{42}$	+++	+
$A\beta_{42}$:$A\beta_{40}$ ratio 1:9	$A\beta_{40}$	+++	+++
	$A\beta_{42}$	+++	+
Pure $A\beta_{40}$	$A\beta_{40}$	NA	+++
	$A\beta_{42}$	NA	+

[a] NA, not applicable.
+, seeding induces aggregation, +++, seeding induces aggregation very efficiently.

induce $A\beta_{40}$ aggregation while at the same time, $A\beta_{40}$ can prevent or delay $A\beta_{42}$ aggregation. Rather than the morphology of the amyloid fibrils, the $A\beta_{42}$:$A\beta_{40}$ ratio modulates the Aβ oligomer formation. Our data indicate that neurotoxicity is more likely to be explained by the dynamic nature of the ongoing Aβ aggregation rather than by the prevailing view that Aβ toxicity is associated with a distinct assembly. A change in the $A\beta_{42}$:$A\beta_{40}$ ratio induces differences in conformational plasticity of the oligomeric peptide mixtures and the pattern of detectable oligomeric species. That the oligomer formation along the amyloid assembly pathway is affected by the different Aβ ratios emphasizes the necessity to further expand our understanding of the exact compositional, temporal, and structural properties of the homo- and hetero-oligomers. The implications of this finding for AD therapy are fundamental: the results imply that it is less important to focus on lowering the total amyloid burden in patients, although it appears crucial to affect the relative ratios of the peptides.

Acknowledgments—We thank the MRC Biomedical NMR centre. We are sincerely indebted with Lesley Calder for generous assistance with TEM analysis. We acknowledge Bart De Strooper for useful discussions.

REFERENCES

1. McLean, C. A., Cherny, R. A., Fraser, F. W., Fuller, S. J., Smith, M. J., Beyreuther, K., Bush, A. I., and Masters, C. L. (1999) Soluble pool of Aβ amyloid as a determinant of severity of neurodegeneration in Alzheimer disease. *Ann. Neurol.* **46,** 860–866
2. Lambert, M. P., Barlow, A. K., Chromy, B. A., Edwards, C., Freed, R., Liosatos, M., Morgan, T. E., Rozovsky, I., Trommer, B., Viola, K. L., Wals, P., Zhang, C., Finch, C. E., Krafft, G. A., and Klein, W. L. (1998) Diffusible, nonfibrillar ligands derived from Aβ1–42 are potent central nervous system neurotoxins. *Proc. Natl. Acad. Sci. U.S.A.* **95,** 6448–6453
3. Klyubin, I., Betts, V., Welzel, A. T., Blennow, K., Zetterberg, H., Wallin, A., Lemere, C. A., Cullen, W. K., Peng, Y., Wisniewski, T., Selkoe, D. J., Anwyl, R., Walsh, D. M., and Rowan, M. J. (2008) Amyloid β protein dimer-containing human CSF disrupts synaptic plasticity: prevention by systemic passive immunization. *J. Neurosci.* **28,** 4231–4237
4. Shankar, G. M., Li, S., Mehta, T. H., Garcia-Munoz, A., Shepardson, N. E., Smith, I., Brett, F. M., Farrell, M. A., Rowan, M. J., Lemere, C. A., Regan, C. M., Walsh, D. M., Sabatini, B. L., and Selkoe, D. J. (2008) Amyloid β protein dimers isolated directly from Alzheimer brains impair synaptic plasticity and memory. *Nat. Med.* **14,** 837–842
5. Lashuel, H. A., Hartley, D., Petre, B. M., Walz, T., and Lansbury, P. T., Jr. (2002) *Nature* **418,** 291
6. Suzuki, N., Cheung, T. T., Cai, X. D., Odaka, A., Otvos, L., Jr., Eckman, C., Golde, T. E., and Younkin, S. G. (1994) An increased percentage of long amyloid β protein secreted by familial amyloid β protein precursor (β APP717) mutants. *Science* **264,** 1336–1340
7. Duff, K., Eckman, C., Zehr, C., Yu, X., Prada, C. M., Perez-tur, J., Hutton, M., Buee, L., Harigaya, Y., Yager, D., Morgan, D., Gordon, M. N., Holcomb, L., Refolo, L., Zenk, B., Hardy, J., and Younkin, S. (1996) Increased amyloid β42(43) in brains of mice expressing mutant presenilin 1. *Nature* **383,** 710–713
8. Scheuner, D., Eckman, C., Jensen, M., Song, X., Citron, M., Suzuki, N., Bird, T. D., Hardy, J., Hutton, M., Kukull, W., Larson, E., Levy-Lahad, E., Viitanen, M., Peskind, E., Poorkaj, P., Schellenberg, G., Tanzi, R., Wasco, W., Lannfelt, L., Selkoe, D., and Younkin, S. (1996) Secreted amyloid β protein similar to that in the senile plaques of Alzheimer disease is increased *in vivo* by the presenilin 1 and 2 and APP mutations linked to familial Alzheimer disease. *Nat. Med.* **2,** 864–870
9. Hellström-Lindahl, E., Viitanen, M., and Marutle, A. (2009) Comparison of Aβ levels in the brain of familial and sporadic Alzheimer disease. *Neurochem. Int.* **55,** 243–252
10. Citron, M., Westaway, D., Xia, W., Carlson, G., Diehl, T., Levesque, G., Johnson-Wood, K., Lee, M., Seubert, P., Davis, A., Kholodenko, D., Motter, R., Sherrington, R., Perry, B., Yao, H., Strome, R., Lieberburg, I., Rommens, J., Kim, S., Schenk, D., Fraser, P., St. George Hyslop, P., and Selkoe, D. J. (1997) Mutant presenilins of Alzheimer disease increase production of 42-residue amyloid β protein in both transfected cells and transgenic mice. *Nat Med* **3,** 67–72
11. Mann, D. M., Iwatsubo, T., Cairns, N. J., Lantos, P. L., Nochlin, D., Sumi, S. M., Bird, T. D., Poorkaj, P., Hardy, J., Hutton, M., Prihar, G., Crook, R., Rossor, M. N., and Haltia, M. (1996) Amyloid β protein (Aβ) deposition in chromosome 14-linked Alzheimer disease: predominance of Aβ42(43). *Ann Neurol* **40,** 149–156
12. Wang, R., Wang, B., He, W., and Zheng, H. (2006) Wild-type presenilin 1 protects against Alzheimer disease mutation-induced amyloid pathology. *J. Biol. Chem.* **281,** 15330–15336
13. Kuperstein, I., Broersen, K., Benilova, I., Rozenski, J., Jonckheere, W., Debulpaep, M., Vandersteen, A., Segers-Nolten, I., Van Der Werf, K., Subramaniam, V., Braeken, D., Callewaert, G., Bartic, C., D'Hooge, R., Martins, I. C., Rousseau, F., Schymkowitz, J., and De Strooper, B. (2010) Neurotoxicity of Alzheimer disease Aβ peptides is induced by small changes in the Aβ42 to Aβ40 ratio. *EMBO J.* **29,** 3408–4320
14. Yoshiike, Y., Chui, D. H., Akagi, T., Tanaka, N., and Takashima, A. (2003) Specific compositions of amyloid β peptides as the determinant of toxic β aggregation. *J. Biol. Chem.* **278,** 23648–23655
15. Jarrett, J. T., and Lansbury, P. T., Jr (1993) Seeding "one-dimensional crystallization" of amyloid: a pathogenic mechanism in Alzheimer disease and scrapie? *Cell* **73,** 1055–1058
16. Bitan, G., Vollers, S. S., and Teplow, D. B. (2003) Elucidation of primary structure elements controlling early amyloid β protein oligomerization. *J. Biol. Chem.* **278,** 34882–34889
17. Chen, Y. R., and Glabe, C. G. (2006) Distinct early folding and aggregation properties of Alzheimer amyloid β peptides Aβ40 and Aβ42: stable trimer or tetramer formation by Aβ42. *J. Biol. Chem.* **281,** 24414–24422
18. Petkova, A. T., Ishii, Y., Balbach, J. J., Antzutkin, O. N., Leapman, R. D., Delaglio, F., and Tycko, R. (2002) A structural model for Alzheimer β amyloid fibrils based on experimental constraints from solid state NMR. *Proc. Natl. Acad. Sci. U.S.A.* **99,** 16742–16747
19. Schmidt, M., Sachse C., Richter, W., Xu, C., Fändrich, M., and Grigorieff, N. (2009) Comparison of Alzheimer Aβ(1–40) and Aβ(1–42) amyloid fibrils reveals similar protofilament structures. *Proc. Natl. Acad. Sci. U.S.A.* **106,** 19813–19818
20. Kirschner, D. A., Abraham, C., and Selkoe, D. J. (1986) X-ray diffraction from intraneuronal paired helical filaments and extraneuronal amyloid fibers in Alzheimer disease indicates cross-β conformation. *Proc. Natl. Acad. Sci. U.S.A.* **83,** 503–507
21. Malinchik, S. B., Inouye, H., Szumowski, K. E., and Kirschner, D. A. (1998) Structural analysis of Alzheimer β(1–40) amyloid: protofilament assembly of tubular fibrils. *Biophys. J.* **74,** 537–545
22. Sikorski, P., Atkins, E. D., and Serpell, L. C. (2003) Structure and texture of fibrous crystals formed by Alzheimer Aβ(11–25) peptide fragment. *Struc-*

ture **11,** 915–926
23. Snyder, S. W., Ladror, U. S., Wade, W. S., Wang, G. T., Barrett, L. W., Matayoshi, E. D., Huffaker, H. J., Krafft, G. A., and Holzman, T. F. (1994) Amyloid β aggregation: selective inhibition of aggregation in mixtures of amyloid with different chain lengths. *Biophys. J.* **67,** 1216–1228
24. Frost, D., Gorman, P. M., Yip, C. M., and Chakrabartty, A. (2003) Co-incorporation of Aβ40 and Aβ42 to form mixed prefibrillar aggregates. *Eur. J. Biochem.* **270,** 654–663
25. Jan, A., Gokce, O., Luthi-Carter, R., and Lashuel, H. A. (2008) The ratio of monomeric to aggregated forms of Aβ40 and Aβ42 is an important determinant of amyloid-β aggregation, fibrillogenesis, and toxicity. *J. Biol. Chem.* **283,** 28176–28189
26. Kim, J., Onstead, L., Randle, S., Price, R., Smithson, L., Zwizinski, C., Dickson, D. W., Golde, T., and McGowan, E. (2007) Aβ40 inhibits amyloid deposition *in vivo*. *J. Neurosci.* **27,** 627–633
27. Yan, Y., and Wang, C. (2007) Aβ40 protects non-toxic Aβ42 monomer from aggregation. *J. Mol. Biol.* **369,** 909–916
28. Broersen, K., Jonckheere, W., Rozenski, J., Vandersteen, A., Pauwels, K., Pastore, A., Rousseau, F., and Schymkowitz, J. (2011) A standardized and biocompatible preparation of aggregate-free amyloid beta peptide for biophysical and biological studies of Alzheimer's disease. *Prot. Eng. Des. Sel.* **24,** 743–750
29. Marshall, K. E., Morris, K. L., Charlton, D., O'Reilly, N., Lewis, L., Walden, H., and Serpell, L. C. (2011) Hydrophobic, aromatic, and electrostatic interactions play a central role in amyloid fibril formation and stability. *Biochemistry* **50,** 2061–2071
30. Makin, O. S., Sikorski, P., and Serpell, L. C. (2007) CLEARER: a new tool for the analysis of x-ray fibre diffraction patterns and diffraction simulation from atomic structural models. *J. Appl. Cryst.* **40,** 966–972
31. Ikura, M., and Bax, A. (1992) Isotope-filtered 2D NMR of a protein-peptide complex: study of a skeletal muscle myosin light chain kinase fragment bound to calmodulin. *J. Am. Chem. Soc.* **114,** 2433–2440
32. Lührs, T., Ritter, C., Adrian, M., Riek-Loher, D., Bohrmann, B., Döbeli, H., Schubert, D., and Riek, R. (2005) Three-dimensional structure of Alzheimer amyloid-β(1–42) fibrils. *Proc. Natl. Acad. Sci. U.S.A.* **102,** 17342–17347
33. Ryu, J., Joung, H. A., Kim, M. G., and Park, C. B. (2008) Surface plasmon resonance analysis of Alzheimer β-amyloid aggregation on a solid surface: from monomers to fully grown fibrils. *Anal. Chem.* **80,** 2400–2407
34. Hou, L., Shao, H., Zhang, Y., Li, H., Menon, N. K., Neuhaus, E. B., Brewer, J. M., Byeon, I. J., Ray, D. G., Vitek, M. P., Iwashita, T., Makula, R. A., Przybyla, A. B., and Zagorski, M. G. (2004) Solution NMR studies of the Aβ(1–40) and Aβ(1–42) peptides establish that the Met-35 oxidation state affects the mechanism of amyloid formation. *J. Am. Chem. Soc.* **126,** 1992–2005
35. Deleted in proof
36. Deleted in proof
37. Deleted in proof
38. Eanes, E. D., and Glenner, G. G. (1968) X-ray diffraction studies on amyloid filaments. *J. Histochem. Cytochem.* **16,** 673–677
39. Makin, O. S., and Serpell, L. C. (2005) Structures for amyloid fibrils. *FEBS J.* **272,** 5950–5961
40. Whittemore, N. A., Mishra, R., Kheterpal, I., Williams, A. D., Wetzel, R., and Serpersu, E. H. (2005) Hydrogen-deuterium (H/D) exchange mapping of Aβ 1–40 amyloid fibril secondary structure using nuclear magnetic resonance spectroscopy. *Biochemistry* **44,** 4434–4441
41. Olofsson, A., Lindhagen-Persson, M., Sauer-Eriksson, A. E., and Ohman, A. (2007) Amide solvent protection analysis demonstrates that amyloid-β(1–40) and amyloid-β(1–42) form different fibrillar structures under identical conditions. *Biochem. J.* **404,** 63–70
42. Wetzel, R., Shivaprasad, S., and Williams, A. D. (2007) Plasticity of amyloid fibrils. *Biochemistry* **46,** 1–10
43. Olofsson, A., Sauer-Eriksson, A. E., and Ohman, A. (2006) The solvent protection of Alzheimer amyloid β-(1–42) fibrils as determined by solution NMR spectroscopy. *J. Biol. Chem.* **281,** 477–483
44. Jan, A., Adolfsson, O., Allaman, I., Buccarello, A. L., Magistretti, P. J., Pfeifer, A., Muhs, A., and Lashuel, H. A. (2011) Aβ42 neurotoxicity is mediated by ongoing nucleated polymerization process rather than by discrete Aβ42 species. *J. Biol. Chem.* **286,** 8585–8596
45. Wogulis, M., Wright, S., Cunningham, D., Chilcote, T., Powell, K., and Rydel, R. E. (2005) Nucleation-dependent polymerization is an essential component of amyloid-mediated neuronal cell death. *J. Neurosci.* **25,** 1071–1080
46. Myszka, D. G., Wood, S. J., and Biere, A. L. (1999) Analysis of fibril elongation using surface plasmon resonance biosensors. *Methods Enzymol.* **309,** 386–402